Journal of the Korean Society of Oceanography
Vol. 39, No. 1, pp. 26 — 34 March 2004

Evolution of suspended sediment patterns in the East China and Yellow Seas

YU-HWAN AHN*, PALANISAMY SHANMUGAM AND SONIA GALLEGOS[1]
Korea Ocean Research and Development Institute, Seoul, 425-600, Korea
[1]*Oceanography Division, Naval Research Laboratory, USA*

The evolution of intricate and striking patterns of suspended sediments (*SS*), which are created by certain physical dynamics in the East China and Yellow Seas, has been investigated using satellite ocean color imageries and vertical profiles of particle attenuation and backscattering coefficients. The structure of these patterns can reveal a great deal about the process underlying their formation. Sea surface temperature (SST) analyzed from the Advanced Very High Resolution Radiometer (AVHRR) thermal infrared data were used to elucidate the physical factors responsible for the evolution of suspended sediment patterns in the East China Sea. The concomitant patterns of suspended sediments were tracked from the Sea-viewing Wide Field-of-view Sensor (SeaWiFS) ocean color data. The detailed examination about these patterns gave birth to the definition of the evolution of suspended sediments (SS) into four stages: (1) Youth or Infant stage, (2) Younger stage, (3) Mature stage, and (4) Old stage. We describe about the three directional forces of the tidal currents, ocean warm currents and estuarine circulations that lead to occurrence of various stages of the evolution of suspended sediments that increase turbidity at high levels through out the water column of the inner and outer shelf areas during September to April. The occurrence of these four stages could be repeatedly observed. In contrast, vertical profiles of the particle attenuation (c_p) and backscattering (b_{bp}) coefficients displayed obvious patterns of the propagation of suspended sediment plume from the southwestern coastal sea that leads to eventual collision with the massive sediment plume originating from the Yangtze banks of the East China Sea.

Key words: Sea WiFS, Ocean Color, Suspended Sediments, Attenuation, Backscattering

INTRODUCTION

The north East China Sea (ECS) is a typical Case-2 water environment receiving a large quantity of land-based materials including nutrients through one of the world's largest river, namely the Yangtze River (He *et al.*, 2000; Yang *et al.*, 2003). It includes a vast and well-developed continental shelf to the northwest, receiving source of energy and material from the Kuroshio, which flows from the south to the northeast along the continental slope of the ECS (Nitani, 1972; Lie *et al.*, 1998 and 2002) (Fig. 1). The shelf waters often form very interesting and beautiful patterns in suspended sediments. These patterns typically arise from the complex interactions between physical, chemical, biological and geological processes (Ahn *et al.*, 2003). Several authors previously observed the existence of such patterns due to tidal currents and estuarine circulations (Yanagi, 1998; Chen, *et al.*, 1995). But, no one has defined the evolution of suspended sediment patterns in the East China Sea or Yellow Sea (YS). We present an extensive analysis to (1) relate the observed patterns to underlying a complex physical processes, (2) characterize and define the evolution of suspended sediments, and (3) characterize the vertical profiles of particle attenuation (c_p) and backscattering (b_{bp}) in relation to the vertical assessment of suspended sediments over these regions. The SeaWiFS and AVHRR imageries covering the southern Yellow Sea and northeast China Sea are used. The optical data acquired by the attenuation and backscatterometers are used to determine the vertical distributions of suspended sediment matter in the southern Yellow Sea.

*Corresponding author: yhahn@kordi.re.kr

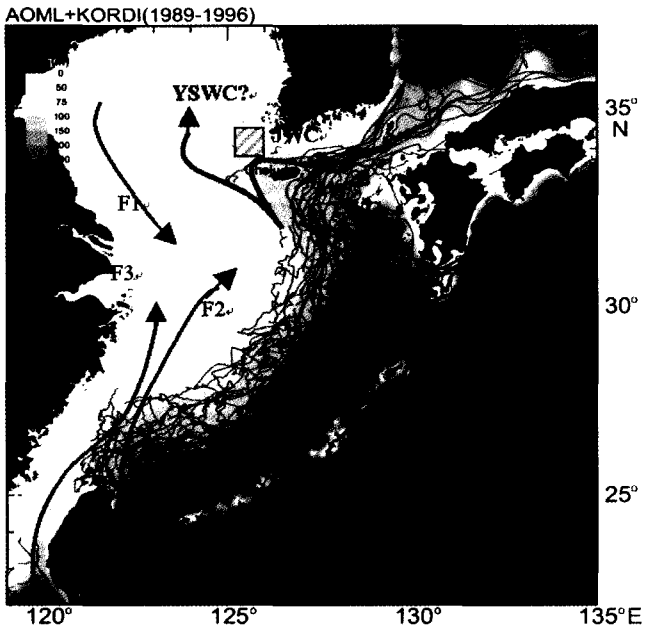

Fig. 1. General patterns in sea surface current field observed from the satellite-tracked drifter trajectories in the East China (a) and Yellow Seas (b) during the period 1989 to 1996. A line-shaded box indicates location of the measurements of particle attenuation and backscattering coefficients.

DATA AND METHODS

The SeaWiFS ocean color instrument flown on Orbview-2, the SeaStar satellite in August 1997 by NASA was specifically designed to provide near-global coverage for every 2 days of upwelled radiance for eight narrow spectral channels (nm) in the visible and near-infrared spectral regions 402-422 (blue), 433-453 (blue), 480-500 (cyan), 500-520 (green), 545-565 (green), 660-680 (red), 745-785 (near-IR), and 845-885 (near-IR) with spatial resolution of 1.13 km (Table 1) (Hooker *et al.*, 1994). Of these, the first six visible channels are used to derive biogeochemical variables (e.g. chlorophyll and suspended sediment concentrations), while the later two near infrared channels centered at 765 and 865nm are used to remove the atmospheric contamination due to aerosol and Raleigh scattering through the atmospheric path and the possible effect of the air-sea interface (Gordon and Wang, 1994). On the other hand, the launches of operational polar orbiting satellites NOAA-12 and 14 have made a major contribution to the ocean climate research in terms of providing global sea surface temperature maps (Donlon *et al.*, 2002). Advanced Very High Resolution Radiometer (AVHRR) flown on these platforms has a spatial resolution of 1.1 km at the nadir, a temporal resolution of approximately six hours (for both the ascending and descending NOAA nodes), and a swath coverage of 2700 km. AVHRR records incoming radiation emitted by the sea surface in two spectral channels (μm) as follows: 10.3-11.3 (μm) and 11.5-12.5 (μm) (Pichel, 1991). The above data sets were highly useful to describe about the physical dynamics and variation of biogeochemical parameters in the East China Sea (Ahn *et al.*, 1999). To estimate SS concentration (g/m^3), we used a single band algorithm (Ahn *et al.*, 2001) rather than adopting a band ratio algorithm because the band ratio algorithm does not perform well in the coastal region, where the DOM absorption is more pronounced towards the shorter wavebands. As a part of this study, vertical profiles of attenuation and backscattering coefficients, c and b_b respectively, at the wavelengths (nm) of 440, 530, 590, and 675 were obtained

Table 1. Characteristic features of the SeaWiFS and AVHRR spectral bands

SeaWiFS			
Spatial Resolution	Spectral Band Specifications		
1.1 km	Band	Wavelength	Color
[Estimates of biogeochemical variables (e.g. Chl and SS)]	1	402-422	Violet
	2	433-453	Blue
	3	480-500	Blue
	4	500-520	Green
	5	545-565	Green
	6	660-680	Red
[Atmospheric correction]	7	745-785	NIR
	8	845-885	NIR
AVHRR (NOAA -12 and 14)			
1.1 km [SST]	4	10.30-11.30,	TIR
	5	11.50-12.50	TIR

in a continuous way by using beam transmissometer and backscatterometers (Wetlabs, Inc.). At these wavelengths, the attenuation coefficients measured were then corrected for the attenuation by pure seawater (particle free) to derive the particle attenuation coefficient, i.e. $c_p = c_t - c_w$. The attenuation coefficient, c_t (λ), can be defined as the sum of $a(\lambda)$ and $b(\lambda)$, namely, $c(\lambda) = a(\lambda) + b(\lambda)$. The c_w accounts for absorption and scattering by water molecules, whereas the c_p is chiefly (~97%) due to particle scattering (Morel and Prieur, 1977). Similarly, the backscattering coefficients were corrected for the backscattering by pure seawater to derive the particle backscattering coefficients (b_{bp}).

SEA SURFACE TEMPERATURE AND OCEANIC CURRENTS

Satellite observations of sea surface temperature (SST) reveal organized patterns of alternate warm and cold-water mass in the boundary zone between the continental shelf and slope areas of the East China and Yellow Seas (Figs. 2a-f). These images corresponded to the SeaWiFS images used in the present study. It is evident that the tide-induced currents transport clod water mass (T=1~7°C) from the Chinese coastal region (north) to the southeast, while the wind-induced currents transport warm water (T=17~29°C) from the south to the northeast through a deeper channel off the continental shelf. The magnitude of these water masses varied with time and space. The southeastward extension of the low saline cold-water mass is the result of the strong tidal currents and converges with the high saline warm-water flowing to the northeast through the southeast shelf edge off the Yangtze river mouth. The three directional forces from the north, south, and west enhances strong lateral mixing at this zone. SST also provides information about the enhanced understanding of the existence of the Jeju Warm Current (JWC), which takes a round clockwise around the Jeju-do at a speed of 3.4~10.8 cm/sec (Lie *et al.*, 2002). It is believed to be a small branch of the Kuroshio. The so-called the Yellow Sea Warm Current (YSWC) remains poorly visible in all SST images, but is often represented by a filament like feature (Ahn *et al.*, 1998).

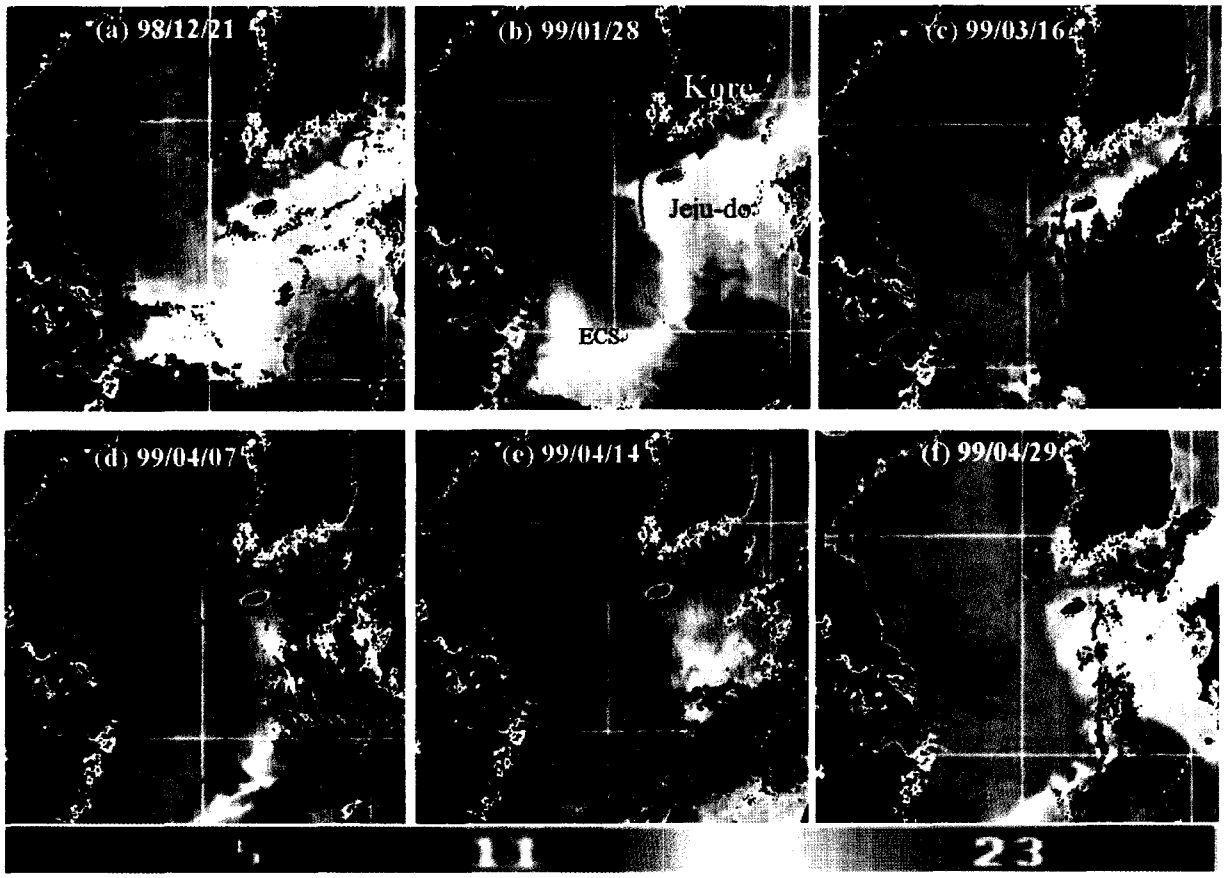

Figs. 2a-f. Spatial and temporal distribution of sea surface temperature and oceanic currents in the East China Sea. EC-East China, ECS-East China Sea, YS-Yellow Sea, YR-Yangtze River.

Table 2. Characteristic features of the evolution of the suspended sediment plume in the East China and Yellow Sea

Characteristics	Origin and Evolution of Suspended Sediments			
	Youth Stage	Younger Stage	Mature Stage	Old Stage
Month	Late September	Middle October - January	Early February middle April	Late April
Location	Confined to a small area to the north of the Yangtze River mouth	Extending to the east of the Yangtze River mouth	Projecting further to the extreme southeast of the Yangtze banks	Localized around the inner part of the Yangtze bank
Area	Several tens of km^2	More than 100 km^2	Several hundreds of km^2	Several tens of km^2
Shape	Barchan	"β	Slender	Longitudinal
Nature of Water	Partially influenced by cold water from the north, and partially by the Yangtze river outflows	The cold water (low saline) from the north begins to dominate the Yangtze river outflows	The cold water (low saline) eventually converge with warm and saline water at the shelf edge	Partially influenced by cold water from the north, and partially by the Yangtze river outflows
Sediment origin	Derived by the river	Partially derived by the river, and partially from sediment resuspnesion by tidal currents.	Sediment resuspnesion dominates river-driven sediments	Mixture of the both origins
Type and Particle size	Silt + Clay PSD <27 μm	Silty clay PSD <35 μm	1. Silty clay with PSD <63 μm limited to the shelf areas on shore 2. Clay particles with PSD <10 μm tend to reach offshore	Clayey silt (PSD<20 μm)
Concentration	SS = <20 g/m^3	SS = <35 g/m^3	SS = >60 g/m^3	SS = <10 g/m^3
Tidal current	Less significant	Significant	Most significant	Less significant
Influence of oceanic currents	Insignificant	Significant	Most significant	Less significant
Sediment trapping	Not visible	Visible	Most Visible	Not Visible
Sediment transport	Not visible	Visible to the southeast of the Yangtze banks	Vigorous and fraternized with the propagation of the JWC	Not visible
Dispersion	Evident	Most evident on the western flanks of the Yellow Sea	Heavy dispersion occurs to the east, and some times to the northwest of the Jeju-do Island due to the YSWC.	Less evident

This filament-like thermal feature often misleads interpreter to the conclusion about the persistent formation of the YSWC (Zheng and Klemas, 1982). Lie *et al.* (2001) also observed a tongue-shaped pattern and described it as an intermittent formation.

EVOLUTION OF SUSPENDED SEDIMENTS IN THE EAST CHINA SEA

We first define the origin and evolution of suspended sediments into four stages based on the number of characteristics common at different stages of the evolution (Table 2). These are seen from their evolution to extinction of suspended sediments. Such characteristics are divided into the stages of: (1) Youth or infant, (2) Younger, (3) Mature, and (4) Old. The resultant patterns are recognizable in the suspended sediment images as shown in Figs. 3a-f.

Youth or Infant Stage

The youth stage of the SS evolution is well characterized by its origin, shape, dimension, particle size, composition, tidal currents, trapping and dispersion. The 'barchan', a small crescent-shaped sediment plume occupy a several tens of square km to the north of Yangtze river mouth and begins to experience the tidal currents generated in the northern parts of the Yangtze banks during late September. At this stage, the sediment plume is closely associated with the low saline cold-water (S< 30 psu and T< 7°C) driven by the large rivers (Σ39,000 m^3/sec) (Chen *et al.*, 2003). However, salinity and temperature have large differences between the upper and bottom layers due to water column stratification (Lie *et al.*, 2002). At this stage, the sediments are thought to be of the terrigeneous origin discharged by the

Yangtze River (332×10^6 ton/yr in 2000) (Yang *et al.*, 2003), and are predominantly composed of equally of silt and clay particles (PSD <27 μm) of illite composition (Youn *et al.*, 2003). The concentration of total suspended sediment matter estimated from the SeaWiFS imagery was maximum of 20 g/m^3. The sediments consist mostly of inorganic particles and may have different shape, size and composition when the tidal currents become more active over these areas (Hill, 1998). The sediment dispersion is obvious even at the weak tidal current on the western flanks of the Yellow Sea. It is interesting to see that the fine clay sediments (PSD <27 μm) exhibit flow patterns on the western flanks of the Yellow Sea, where the high saline water (S >34 psu) acts as carrier to transport the fine sediments offshore (Fig. 3a). Due to weak tidal current, the transport of mobile sediments in the bottom layers may be limited to the shelf areas.

Younger Stage

The "β" shaped plume represents the younger stage, which beings to appear in middle October and continues until January (Fig. 3b). The aerial extent of this plume increases significantly to several hundreds of square km to the east of the Yangtze river mouth and increases further to the western flanks of the Yellow Sea, where the fine clay sediments (PSD <35 μm) often form flow patterns off the Yangtze banks. The evolution of this stage is primarily governed by the two-directional forces acting upon the plume formation from the north by the tidal currents and from the west by the Yangtze River. At this stage, the water column responds rapidly to the cold water mass changing from stratified (with respect to salinity, temperature and suspended sediment) to well-mixed state, resulting in high-suspended sediment concentration (SS<35 g/m^3) throughout the water column. The SST and SS images apparently show that tidal currents associated with surface waves cause resuspension greatly throughout the inner shelf areas during December (Figs. 2a and 3b). Consequently, the sediment composition and particle size change to the silty clay type (PSD <35 μm), where the silt particles seem to have higher population than the clay particles. The strong northerly prevailing winds

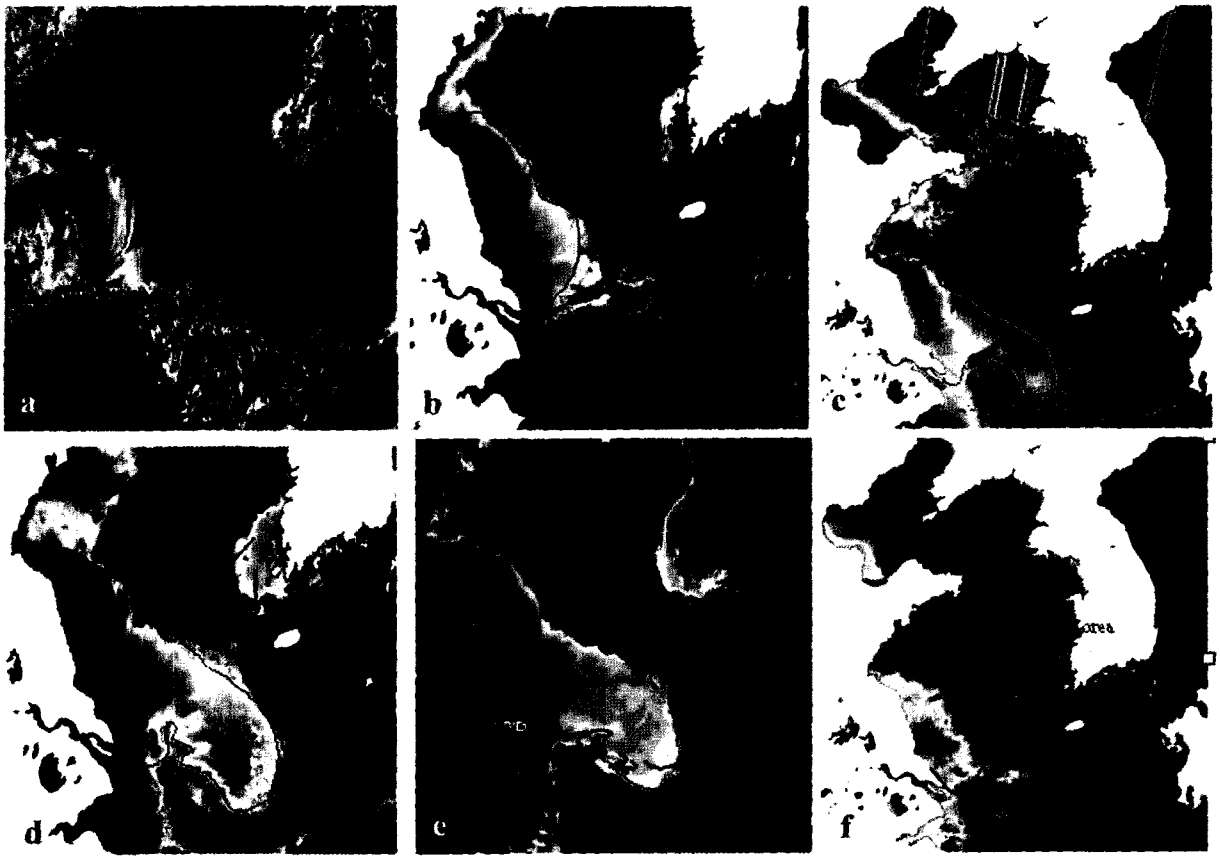

Figs. 3a-f. Evolution of suspended sediment plume in the East China and Yellow Seas during November 1998 to April 1999. (a) Youth Stage, (b and c) Younger Stage, (d & e) Mature Stage, (f) Old Stage. DD-Dispersion direction; MD-Moving direction; DW-Deep water; SSP- Suspended sediment plume.

pushes the low saline water from the northeast China shelf to the southeast, leading to prevail decreased salinity (S<31 psu) and temperature (T<5°C). As the tidal currents progresses, the bottom accumulated mobile sediments get resuspended and appear to overflow off the western flanks of the Yellow Sea. The southeastward bottom topography and the prevailing winds from the north result in trapping of mobile sediments onto a frontal zone existed at the shelf edge to the southeast off the river mouth. The sediments trapped at the depth greater than 60 m increase vertical and horizontal stability of flow around the banks. These sediments may often exhibit particle aggregation, disaggregation and flocculation due to the combined effect of estuary circulation and tidal currents, leading to produce poorly sorted mixed particles (Hill, 1998). At this stage, more emphasis is placed on the tidal currents rather than the oceanic warm currents. The well-mixed suspended sediments due to strong tidal currents encounter essential frontal trapping at the east and the extreme southeast shelf edge of the ECS.

Mature Stage

The mature stage is recognized by a "slender" like pattern of sediment plume corresponding to a broad continental shelf areas and occupies a thousands of sq. km from the northeast to the extreme southeast of the Yangtze banks (Fig. 3d and e). It eventually encounters three directional forces generated by tidal currents from the north, oceanic currents from the south and the river outflows from the west as illustrated in Fig. 1. These forces as represented by F1, F2 and F3 can be distinguished based on their nature of influence on the sediment plume. During this stage, the northerly prevailing winds that blow across the Yellow and East China Seas generate large waves that enter the Yangtze banks from the north, leading to produce very high turbidity throughout the shelf areas. The strong tidal currents associated with these waves cause the sediment resuspension greatly at a water depth 60 m over the areas exposed to the southeast (Fig. 3d). At this stage, the tide-induced resuspension of sediments produce concentrations over 60g/m^3 and are not compensated by sediments discharged by the river. Moreover, the Yangtze river discharge decreases greatly during middle and late winter (Lie *et al.*, 2001), and the strong bottom turbulence associated with the tidal currents results in large increases in concentration of sediments relative to the riverine source (Ahn *et al.*, 2003). Sediment trapping in frontal zones, both in estuary and on the inner shelf to the southeast, increases the concentration of sediments to a greater extent throughout the shelf areas. In certain situation, that is at high concentrations, the density anomaly due to the sediment itself contributes to the vertical stability of the flow, increasing the trapping efficiency of the frontal zone. This would lead to high concentrations within the shelf areas of the order of several cm thick, and may often represent an important cross-shelf conduit of sediments. This is one of the major events in the ECS, but has not been observed before. The high concentration of sediment layers formed by frontal trapping can attain excess densities large enough to initiate down slope motion on the continental shelf to the southeast of the river mouth, resulting in an important cross-shelf transport both at surface and deep waters. The three directional forces can explain such transport. The sediment aggregation, disaggregation and flocculation are the most evident processes during the evolution of younger stage, producing variable grain size, shape, composition and concentrations. From the data gathered, it can be said that the coarse sediment particles dominate the shelf areas (PSD <63 μm), while the fine clay particles (PSD <10 μm) dominate and appear to follow the direction of the propagation of the Jeju Warm Current (Ahn *et al.*, 2003), which takes a round clockwise around the Jeju-do with an average distance of about 25-30 km (Fig. 3e). One of the major considerations here is that the density difference between riverine and salt water as well as the density anomaly contributed by sediment have important consequences on the transport of sediment issued from the land and seabed. Sediment transport and dispersion is the most important phenomenon that resolves the controversial problem of the existence of the YSWC. In contrast to the younger stage, the transported fresh and cold water mass (S< 30 psu and T< 7°C) to the extreme southeast off the Yangtze banks can undergo changes in its physical state owing to the influence of oceanic warm currents (S >32 psu and T> 10°C) at the shelf edge.

Old Stage

The old stage exhibits longitudinal pattern of suspended sediment plume, covering an area of a several tens of square kilometer. It lays parallel to the coast to the northeast of the Yangtze River mouth (Fig. 3f). It begins to experience variable wind directions

and weakening of northerly prevailing winds in late April (Han *et al.*, 1995). During this time, the Yangtze river begins to discharge a large volume of fresh water including nutrients to the coastal system, which, in turn, results in displacing mixed water localized on the western flanks of the Yellow Sea. According to Jacobs *et al.* (2000), the prevailing southern wind may play a major role in displacing and transporting the mixed water mass to the east off the banks. The geographical area of fresh water regime (S< 29 psu) constantly increases to the east and further northeast off the river mouth until the beginning of the youth stage in late September. The weak tidal currents yield sediment concentration SS = <10 g/m^3 with PSD<20 μm and transforms the SS plume to a stratified form during summer monsoon Lie *et al.* (2002). The sediment trapping is not evident at this stage. The large volume of river discharge produces the dominant pathway of terrigeneous sediments to the shelf areas to the northeast of the river mouth (Yang *et al.*, 2003).

OPTICAL CHRACTERIZATION OF SUSPENDED SEDIMENT

Vertical profiles of particle attenuation (c_p=c_t-c_w) and backscattering (b_{bp}=b_b-b_{bw}), at four wavelengths (nm) 440, 530, 590, and 675, were measured using attenuation and backscatterometers to describe about the vertical distribution of suspended sediment matter caused by strong tidal currents from the southwest coastal regions of Korea. Previous studies demonstrated the usefulness of these coefficients that are well correlated with the concentration of total suspended particulate matter (Loisel and Morel, 1998, Gardner *et al.*, 1985). Therefore, the vertical variations of particulate attenuation (c_p), backscattering (b_{bp}) allowed the sample sites to be characterized with respect to the distribution of suspended sediment matter (Figs. 4a-c). Both coefficients covaried through out the vertical column of water at all stations. Voss (1992) observed that there is a linear relationship existed between the particulate attenuation at the blue and red wavelengths. Compared to all other wavelengths, the coefficients of c_p and b_{bp} are much higher at 440 nm. Note that particle attenuation (c_p) and backscattering (b_{bp}) coefficients at station 310-10B (sampled on June 1996) remained weak (0.6 and 0.005 m^{-1} respectively) in the upper layer around 0-48 m and progressively increased to 2.4 and 0.045 m^{-1} in the deep layer confined to sediment maximum at 48-61 m (Figs. 4a1 and a2). Such patterns allow us to conclude that the water column became vertically stratified and the previously resuspended sediment materials appeared to have settled down to the deep layer (Figs. 4a1 and a2).

In contrast, a good evident has been gathered to show suspended sediments propagating from the southwest coastal area to the southern Yellow Sea. At station 312-4A (sampled on November 1996 inshore), c_p and b_{bp} values exhibit a steady increase through out the profiles, reaching a maximum of 10 m^{-1} and 0.4 m^{-1} respectively (Figs. 4b1 and b2). The high values of particle attenuation and backscattering coefficients are directly related to the increase of suspended sediment concentration caused by tidal currents and enhanced bottom circulations. At station 312-5A, vertical profiles displayed four distinct layers with a sharp deep maximum at 11 m, 23 m, 57 m and 62 m respectively (Figs. 4c1 and c2). The low values of c_p and b_{bp} respectively, 0.5 m^{-1} and 0.02 m^{-1}, corresponded to the surface layer from 0 to 11 m. However, the c_p and b_{bp} increased sharply (3.8 m^{-1} and 0.07 m^{-1} respectively) at the depth of 11-23 m and tended to stabilize at 23-57 m, due to a constant flow of turbid plume at this layer. There were two distinct peaks at 25 and 45 m attributable to algal matter. One should note that the very high attenuation (c_p) and backscattering (b_{bp}) coefficients (7.5 and 0.23 m^{-1} respectively) at 57-62 m were likely due to down-slope due to propagation of massive sediment plume composed of high proportion of poorly sorted intermediate and coarse particles caused essentially by strong tidal currents and bottom circulations. From the analysis, we confirm the propagation of massive sediment plume with the help of vertical attenuation and backscattering coefficients of light, which are obviously related to the total suspended particulate matter (Loisel and Morel, 1998; Boss *et al.*, 2001).

CONCLUSIONS

The analysis of satellite ocean color imageries and SST allowed us to describe the evolution of complicate and striking patterns of suspended sediment in the East China and Yellow Seas. The maps of suspended sediment matter derived from the SeaWiFS ocean color imageries gave special emphasis on the evolution of suspended sediments into various stages, while retrieval of SST from AVHRR thermal infrared data were found to be useful in demonstrating the

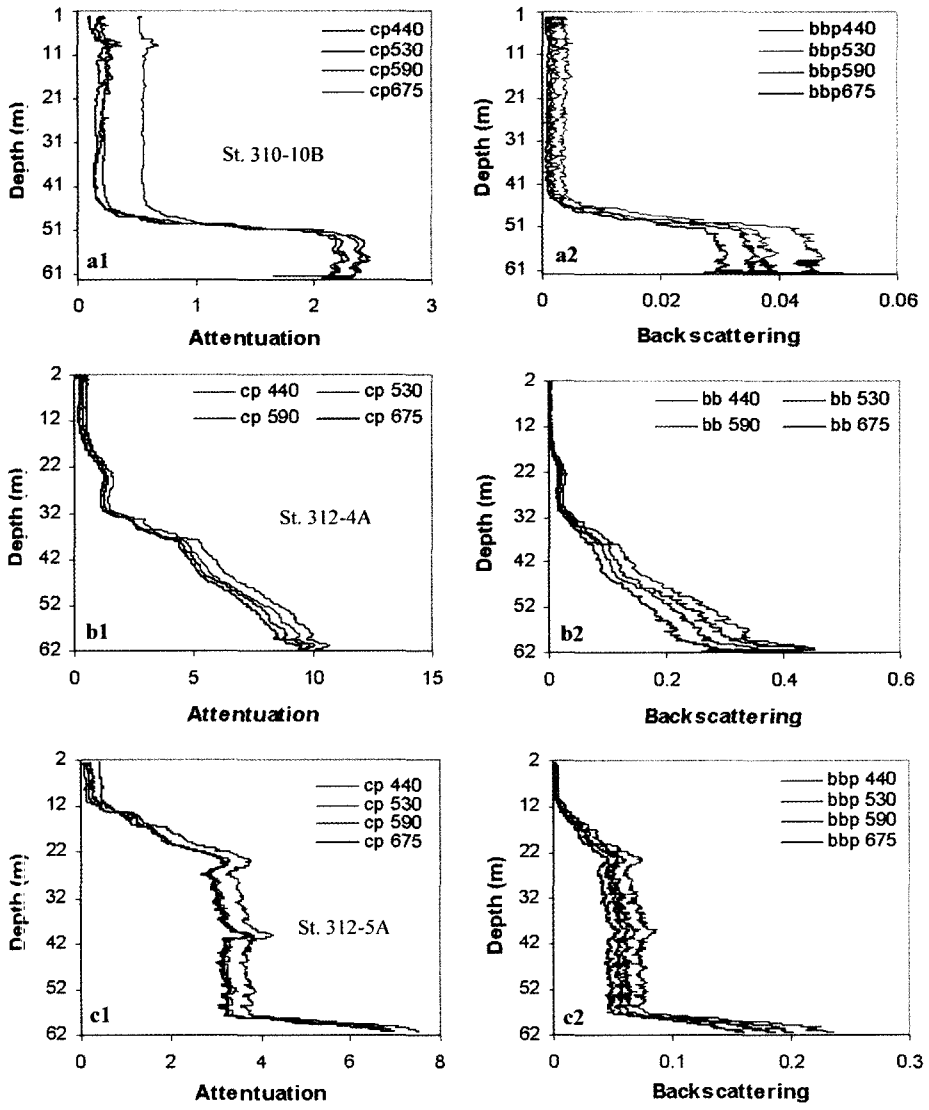

Figs. 4a-c. Vertical profiles of particle attenuation and backscattering coefficients showing patterns of suspended sediment matter in the southern Yellow Sea.

movement of cold and warm water masses resulted from various physical dynamics of the East China Sea. No previous study gave special attention to examine and define the evolution of suspended sediments of the East China Sea. It was evident that the magnitude of suspended sediment plume appeared to be constantly increased from youth stage to mature stage of the period September to February and reached the extinction stage during April. The three directional forces that result from the tidal currents, oceanic warm currents and estuarine circulation could explain the development of each stages of SS evolution, leading to produce very high turbidity over the East China and Yellow Seas. From this study, it is thought that the occurrence of cross shelf transport of the plume of massive sediments could be important in several aspects and only be elucidated by measuring vertical profiles of particle attenuation (c_p) and backscattering coefficients (b_{bp}). We presented several examples of vertical profiles of particle attenuation and backscattering coefficients measured in the southern Yellow Sea. The values of these coefficients rapidly increased with depth were closely associated with currents moving from inshore to offshore. The attenuation and backscattering coefficients are two orders of magnitude higher than those observed in the southern central part of the Yellow Sea. We believe that integration of real time data sets consisting of satellite ocean color imagery, suspended sediment concentrations, particle size distributions (PSD), particle attenuation and backscattering coefficients and surface currents fields would enhance better understanding of the surface and subsurface sediment climatology of the East Chin Sea and Yellow Sea.

ACKNOWLEDGEMENTS

This research was partially supported by MOST and MOMAF under KORDI research projects PN50900, PG37400 and PM21800, respectively. The NRL work was supported by the NRL-CORE Project "Coupling of sediment and optical models". We thank NFRDI for providing some of the CTD data used in this study.

REFERENCES

Ahn, Y.H., S. Gallegos and R. Iturriaga, 1998. The influence of resuspended sediment particles on the ocean color algorithm. *Proceeding of Ocean Optics XIV Meeting* in Hawaii.

Ahn, Y.H., H.J. Lie and J.E. Moon, 1999. Variations of water turbidity in Korean waters. *Proceeding of the International symposium on Progress in Coastal Engineering and Oceanography*, Seoul, Korea

Ahn, Y.H., J.E. Moon and S. Gallegos, 2001. Development of suspended particulate matter algorithms for ocean color remote sensing. *Korean Journal of Remote Sensing*, **17**: 285–295.

Ahn, Y.H., P. Shanmugam., H.J. Lie and J.E. Moon, 2003. Characterization of the Moving Direction and Diffusion of the East China coastal waters by ocean color satellite, *Proceedings of the Spring Meeting, 2003 of the Korean Society of Oceanography*, Cheju, Korea

Boss, E., M.S. Twardowski and S. Herring, 2001. Shape of the particulate beam attenuation spectrum and its inversion to obtain the shape of the particulate size distribution. *Applied Optics*, **40**: 4885–4893.

Bricaud, A., C. Roesler and J.R.V. Zaneveld, 1995. In situ methods for measuring the inherent optical properties of ocean waters. *Limnology and Oceanography*, **40**: 393–410.

Chen, C., J. Zhu., R.C. Beardsley and P.J.S. Franks, 2003. Physical-biological sources for dense algal blooms near the Changjiang River. *Geophysical Research Letter*, **30**: 22.1–22.4.

Chen, C., A. Ruto., S.C. Pai., C.T. Liu and G.T.F. Wong, 1995. Exchange of water masses between East China Sea and the Kuroshio off northern Taiwan. *Continental Shelf Research*, **15**: 19–39.

Donlon, C.J., P.J. Minnett., C. Gentemann., T.J. Nightingale., I.J. Barton., B. Ward and Murray. 2002. Toward improved validation of satellite sea surface skin temperature measurements for climate research. *Journal of climate*, **15**: 353–369.

Garnder, W.D., P.E. Biscaye., J.R.V. Zaneveld and M.J. Richardson 1985. Calibration and comparison of the LDGO nephelometer and the OSU transmissometer on the Nova Scotian Rise. *Marine Geology*, **66**: 323–344.

Gordon, H.R. and M. Wang, 1994. Retrieval of water-leaving radiance and aerosol optical thickness over the oceans with SeaWiFS: a preliminary algorithm. *Applied Optics*, **33**: 443–452.

Han, S.K., H.J. Lie and J.Y. Na, 1995. Temporal and spatial characteristics of surface winds over the adjacent seas of the Korean peninsula. *Journal of Korean Society of Oceanography*, **30**: 550–564.

He, M.X., Z.S. Liu., K.P. Du., L.P. Li., R. Chen., Carder and Z.P. Lee, 2000. Retrieval of chlorophyll from remote sensing reflectance in the East China Seas. *Applied Optics*, **39**: 2467–2474.

Hill, P.S., 1998. Controls on floc size in the coastal ocean. *Oceanography*, **11**: 13–18

Hooker, S.B., E.R. Firestone and J.G. Acker, 1994. SeaWiFS Prelaunch Radiometric Calibration and Spectral Characterization. SeaWiFS technical report series, NASA Technical Memorandum 104566, Vol. 23.

Jacops, G.A., H.B. Hur and S.K. Riedlinger, 2000. Yellow and East China Seas response to winds and currents. *Journal of Geophysical Research*, **105**: 21947–21,968.

Lie, H.J. and C.H. Cho, 2002. Recent advances in understanding the circulation and hydrography of the East China Sea, *Fisheries Oceanography*, **11**: 318–328.

Lie, H.J., C.H. Cho., J.H. Lee and S. Lee, 2001. Does the Yellow Sea Warm Current really exist as a persistent mean flow? *Journal of Geophysical Research*, **106**: 199–210.

Loisel, H. and A. Morel, 1998. Light scattering and chlorophyll concentration in case-1 waters: A reexamination. *Limnology and Oceanography*, **43**: 847–858.

Morel, A. and L. Priuer, 1977. Analysis of variations in ocean color. *Limnology and Oceanography*, **22**: 709–722.

Nitani, H., 1972. Beginning of the Kuroshio. In Kuroshio. H. Stommel and K. Yoshida (eds). Tokyo: University of Tokyo Press, 353–369.

Pichel, W.G., 1991. Operational production of multichannel sea surface temperatures from NOAA polar satellite AVHRR data. *Palaeogeography, Palaeoclimatology, Palaeoecology*, **90**: 173–177.

Reilly, J.E., S. Maritorena., B.G. Mitchell., D.A. Seigel., K.L. Carder., S.A. Garver., M. Kahru and C. McClain, 1998. Ocean color chlorophyll algorithms for SeaWiFS. *Journal of Geophysical Research*, **103**: 24,937–24953.

Yang, S.L., I.M. Belkin., A.L. Belkina., Q.Y. Zhao., J. Zhu and P.X. Ding, 2003. Delta response to decline in sediment supply from the Yangtze River: evidence of the recent four decades and expectations for the next half-century. *Estuarine, Coastal and Shelf Science*, **57**: 689–699.

Yanagi, T., 1998. Hydrographic material transport, budget and ecological models in the East China Sea. *Bull. Coastal Oceanography*, **36**: 59–68.

Manuscript received October 15, 2003
Revision accepted February 15, 2004
Editorial handling: Tetsuo Yanagi